Effect of integral membrane proteins on the lateral mobility of plastoquinone in phosphatidylcholine proteoliposomes

Mary F. Blackwell and John Whitmarsh
Photosynthesis Research Unit, United States Department of Agriculture/Agricultural Research Service; and Department of Plant Biology, University of Illinois, Urbana, Illinois 61801 USA

ABSTRACT Pyrene fluorescence quenching by plastoquinone was used to estimate the rate of plastoquinone lateral diffusion in soybean phosphatidylcholine proteoliposomes containing the following integral membrane proteins: gramicidin D, spinach cytochrome *bf* complex, spinach cytochrome *f*, reaction centers from *Rhodobacter sphaeroides*, beef heart mitochondrial cytochrome bc_1, and beef heart mitochondrial cytochrome oxidase. The measured plastoquinone lateral diffusion coefficient varied between 1 and $3 \cdot 10^{-7}$ cm^2 s^{-1} in control liposomes that lacked protein. When proteins were added, these values decreased: a 10-fold decrease was observed when 16–26% of the membrane surface area was occupied by protein for all the proteins but gramicidin. The larger protein complexes (cytochrome *bf*, *Rhodobacter sphaeroides* reaction centers, cytochrome bc_1, and cytochrome oxidase), whose hydrophobic volumes were 15–20 times as large as that of cytochrome *f* and the gramicidin transmembrane dimer, were 15–20 times as effective in decreasing the lateral-diffusion coefficient over the range of concentrations studied. These proteins had a much stronger effect than that observed for bacteriorhodopsin in fluorescence photobleaching recovery measurements. The effect of high-protein concentrations in gramicidin proteoliposomes was in close agreement with fluorescence photobleaching measurements. The results are compared with the predictions of several theoretical models of lateral mobility as a function of integral membrane concentration.

INTRODUCTION

Ever since Singer and Nicolson proposed the fluid mosaic model of membranes (1), it has been of interest to determine how membrane fluidity affects cell function. A number of systems in which lateral mobility may play a functional role have been identified (2, 3). Methods for measuring membrane viscosity and lateral mobility of membrane proteins and lipids have been developed and used extensively to study transport properties in biological membranes (2, 4–10). These methods include fluorescence photobleaching recovery (FPR) (4, 9, 10) and probe fluorescence quenching (5–8). Some studies have focused on the lateral mobility of quinone molecules because of their function as mobile substrates for quinol-cytochrome oxidoreductases (3, 5–10). It was unclear whether quinones, whose isoprenoid tails and headgroup characteristics differ from those of acyl lipids, would occupy a special membrane milieu with accompanying effects on their mobilities (3, 5–11). Quinone diffusion coefficients in the region of $1–3 \cdot 10^{-7}$ cm^2/s measured in liposomes by the probe fluorescence–quenching technique (6–8) are closer in value to those of other lipids (2, 4, 9, 12, 14) than values $>10^{-6}$ cm^2 s^{-1} that were initially calculated from fluorescence-quenching measurements (6, 7). The higher values were calculated before it was determined that transient dynamic quenching in membranes makes a significant, sometimes dominant, contribution to fluorescence quenching in membranes and needs to be taken into account in the calculation of diffusion coefficient (8).

Biological membranes are generally associated with significant amounts of protein, ranging from about 20 wt% protein for myelin to over 70 wt% protein for chloroplast lamellae, *Halobacterium* purple membrane, and mitochondrial inner membrane (e.g., 13). Measurements of lipid diffusion by FPR in proteoliposomes containing bacteriorhodopsin (14) or gramicidin (15) indicated that lateral diffusion is dramatically reduced in the physiologically meaningful region of protein concentrations. Both analytical and numerical models have been developed to predict the effect of integral membrane proteins on lateral mobility in membranes. The analytical theories of lipid mobility include models in which diffusion is considered to be a random walk process on a lattice of points or disks (16–18), which we shall refer to as lattice models, a free volume model (19), and models that consider that lipids immediately surrounding proteins or trapped between protein molecules may have restricted mobility, which we shall refer to as lipid domain models (20). Numerical studies of lateral mobility (17, 21–23) consist primarily of Monte Carlo simulations. Two recent analytical theories of Brownian motion for proteins in membranes (24, 25) may prove applicable to lipids. The

Dr. Blackwell's present address is Department of Chemistry, Lawrence University, Appleton, WI 54912.

lattice models, which include percolation and effective medium theories (16–18), are in good agreement with the results of Monte Carlo calculations but predict a weaker dependence of lipid diffusion rates on the protein concentration than was observed experimentally (14, 15). This is consistent with the finding that diffusion coefficients from Monte Carlo calculations are not in agreement with experimental values at high protein concentrations unless protein/protein or lipid/protein interactions are included in the calculation (21–23).

The aim of the present paper is to provide a systematic experimental investigation of lateral mobility as a function of the protein content in model membrane systems in which the protein composition can be controlled and quantitated. The pyrene fluorescence–quenching technique (8) was used to study how plastoquinone lateral diffusion depends on the protein concentration in soybean phosphatidylcholine proteoliposomes containing six integral membrane proteins: gramicidin D, spinach cytochrome *bf* complex, and cytochrome *f*, reaction centers from *Rhodobacter sphaeroides*, and the cytochrome bc_1 and cytochrome oxidase complexes from beef heart mitochondria.

A preliminary account of this work has been presented (26).

MATERIALS AND METHODS

Pyrene, soybean phosphatidylcholine (type III-S, ~99%), sodium cholate, β-octyl glucoside, and gramicidin D were used as purchased from Sigma Chemical Co. (St. Louis, MO). Nonanoyl-*n*-methylglucamide (MEGA-9) detergent was synthesized by a published procedure (27). Plastoquinone-9 was a gift from Hoffman-La Roche (Basel, Switzerland). *Rhodobacter sphaeroides* R-26 reaction centers were a gift from Dr. Colin Wraight, prepared by the procedure of Maroti and Wraight (28). Cytochrome *f* (29) and cytochrome *bf* complex (30) from market spinach, and cytochrome oxidase (31) and cytochrome bc_1 complex (31) from beef heart mitochondria were isolated by published procedures and had the following characteristics: 120 g protein per mol cytochrome *f* in the cytochrome *bf* complex; 38 g per mol cytochrome *f* in purified cytochrome *f*; 180 g per mol cytochrome aa_3 in cytochrome oxidase; and 287 g per mol cytochrome c_1 in cytochrome bc_1 complex. When necessary, proteins were concentrated to 5–20 mg/ml protein by dialysis for several hours against 22% polyethylene glycol in a buffer solution (50 mM Tris-HCl, pH 8 (5°C)) containing 3% sodium cholate, followed by overnight dialysis against a buffer solution (10 mM Tris-HCl, pH 8 (5°C)) containing 1% sodium cholate. Unless stated otherwise, all steps were carried out at 0–5°C.

Solid plastoquinone was dissolved in *n*-hexane and then diluted with absolute ethanol. Plastoquinone concentrations in ethanol and cytochrome aa_3, *f*, and c_1 concentrations were determined using published extinction coefficients (32–35). Oxidized minus reduced cytochrome absorbance spectra were measured on a SLM-Aminco DW-2C spectrophotometer (SLM Instruments, Urbana, IL). Protein concentrations were estimated by the method of Bensadoun and Weinstein (36).

Plastoquinone diffusion coefficients were estimated by the pyrene fluorescence–quenching method (8), which involves measurements of steady-state pyrene fluorescence emission intensities as a function of the plastoquinone concentration. The lipid/pyrene ratio was kept >100 to avoid significant steady-state pyrene excimer fluorescence (37). The plastoquinone concentration was kept <1 mM in the membrane (as defined in Eq. A1 or A3 of Appendix A) to avoid nonlinearity in Stern-Volmer plots observed previously (8), believed to be due to limited plastoquinone solubility in lipid bilayers. Plastoquinone-9 could not be incorporated into aqueous suspensions of preformed membranes in the absence of detergent (data not shown); thus, two methods were used to construct proteoliposomes containing plastoquinone, as follows.

Method A. Plastoquinone incorporation by detergent dilution

Appropriate volumes (10–100 μl) of stock solutions of pyrene (0.124 mg/ml) and phosphatidylcholine (100 mg/ml) in chloroform and of plastoquinone in 95% ethanol/5% hexane were mixed in 12 × 75-mm glass culture tubes, dried to a thin film under a stream of nitrogen and then vortexed to clarity in a solution of 2% MEGA-9 in distilled water. Usually, six such solutions were made up, corresponding to five different concentrations of plastoquinone (including zero) and one blank sample containing phosphatidylcholine, but no pyrene or plastoquinone. For each weight percent protein, aliquots of the latter solutions were combined with appropriate amounts of protein in buffer solution (10 mM Tris-HCl, pH 8 [5°C]) containing 1% sodium cholate, followed by dilution to 2 ml with buffer solution. The detergent concentration was made equal in all of the samples. The final concentrations were 0.1 or 0.2 mg/ml lipid and 0.3–0.5 μM pyrene, as noted in the figure captions. The final detergent concentrations, typically 1 mM MEGA-9 and 1.2 mM sodium cholate, were more than an order of magnitude lower than the critical micellar concentrations, 15 mM for MEGA-9 (38) and 14 mM for cholate (39). A reasonable estimate for the combination of 1 mM cholate and 0.1–0.2 mg/ml phosphatidylcholine is a lipid/detergent molar ratio in the bilayer phase of 5–10, assuming a lipid/water partition coefficient for cholate similar to that reported for glycocholate in egg phosphatidylcholine (40) and a lipid density 1 g/ml (41, 42). Both the diffusion coefficients and the membrane morphology, unilamellar vesicles with a diameter of about 100 nm observed by negative stain electron microscopy (data not shown), were similar to those observed in control studies with unilamellar vesicles prepared by sonication that did not contain detergent (data not shown).

Method B. Plastoquinone incorporation by liposome fusion

Proteoliposomes containing 80% of the total lipid were prepared as follows. Appropriate volumes (10–100 μl) of stock solutions of pyrene (0.124 mg/ml) and phosphatidylcholine (100 mg/ml) in chloroform in 12 × 75-mm glass culture tubes, dried to a thin film under a stream of nitrogen and then vortexed to clarity in a solution of 2% MEGA-9 in distilled water. For each weight percent protein, aliquots of the latter solutions were combined with appropriate amounts of protein in buffer solution (10 mM Tris-HCl, pH 8 (5°C)) containing 1% sodium cholate, followed by dilution to 2 ml with buffer solution. The detergent was removed by dialysis against 500 vol of 10 mM Tris-HCl (pH 8, 5°C), with one change of dialysis buffer. Plastoquinone was incorporated with the remaining 20% lipid as follows. Plastoquinone-containing liposomes were prepared by combining appropriate volumes of lipid and plastoquinone in organic stock solutions, drying under a stream of nitrogen, and dispersing into distilled water by ultrasonic irradiation for 10 s at 26 μm using a MSE Soniprep 150 Ultrasonic Disintegrator (MSE Scientific Instruments, Crawley, Sussex, UK) with an exponential microtip. Plastoquinone-containing liposomes were fused with proteoliposomes by

ultrasonic irradiation (10 s at 26 μm) followed by 0–2 freeze-thaw cycles. The inclusion of freeze-thaw cycles did not affect the results.

Steady-state measurements of pyrene fluorescence were carried out on an SLM-Aminco SPF-500 spectrofluorometer (SLM Instruments, Urbana, IL) at room temperature (22–24°C) in a 1 cm^2 quartz cuvette. Emission was measured at 390 nm (bandpass 10–20 nm) with excitation at 330 nm (bandpass 1–4 nm). A blank value of fluorescence from proteoliposome samples that lacked pyrene or plastoquinone, but were otherwise identical, typically 10% or less, was subtracted. Fluorescence kinetics were measured at 390 nm with excitation at 330 nm on a single–photon counting nanosecond fluorimeter (PRA Associates, Inc., London, Ontario, Canada) in the laboratory of Dr. L. Faulkner, Urbana, IL. The nonlinear least-squares analysis of pyrene monomer fluorescence decay kinetics was described previously (8, 37).

RESULTS

Pyrene fluorescence quenching by plastoquinone in proteoliposomes

In Stern-Volmer plots, steady-state probe fluorescence emission intensity ratios, I^0/I, are plotted as a function of the concentration of a quencher, where I^0 and I are the respective intensities in the absence and presence of quencher. Fig. 1 shows Stern-Volmer plots with pyrene as the probe and plastoquinone as the quencher in phosphatidylcholine proteoliposomes containing a constant concentration of phosphatidylcholine (0.1 mg/ml) and variable amounts of spinach cytochrome *bf* complex, prepared by the detergent dilution technique (Method A). Stern-Volmer plots are shown for liposome samples containing no protein (Fig. 1, *top trace*) and in proteoliposome samples containing successively higher contents of cytochrome *bf* complex (Fig. 1, *top to bottom*) ranging from 14 to 62 wt% protein (defined here as grams of protein per total grams of protein and lipid added to the samples). It is evident in Fig. 1 that the slope of I^0/I vs. plastoquinone concentration decreases as the protein concentration increases, indicating a decrease in the extent of pyrene fluorescence quenching in the presence of integral membrane proteins. All six of the integral membrane proteins studied resulted in large decreases in pyrene fluorescence quenching by plastoquinone in the region of 10–60 wt% protein (data not shown), similar to those shown in Fig. 1. The decrease in fluorescence quenching in proteoliposomes will be assumed to correspond to a decrease in the rate of encounters between plastoquinone and pyrene and, hence, to a decrease in lateral mobility. Other possible causes of the decrease are mentioned in the Discussion.

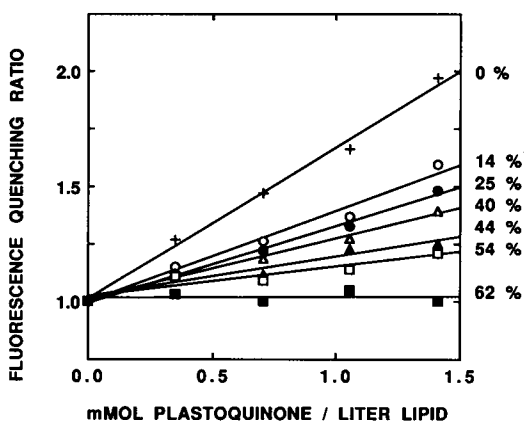

FIGURE 1 Pyrene fluorescence quenching in soybean phosphatidylcholine proteoliposomes at different weight percentages of spinach cytochrome *bf* complex. Stern-Volmer plots of the pyrene fluorescence intensity ratio I^0/I, as a function of the plastoquinone concentration in proteoliposomes containing spinach cytochrome *bf* complex at (*top to bottom*) 0, 14, 25, 40, 44, 54, and 62 wt% protein, with I^0 and I the respective fluorescence emission intensities measured in the absence and presence of plastoquinone. Steady-state fluorescence emission at room temperature (24°C) was measured at 390 nm with excitation at 330 nm. A blank value of fluorescence from proteoliposomes that lacked both pyrene and plastoquinone was substracted from I^0 and I. The phosphatidylcholine concentration was 0.1 mg/ml, and the pyrene concentration was 0.3 μM in a buffer solution of 10 mM Tris-HCl (pH 7.5). The proteoliposomes were prepared by Method A. Further details are given in the text.

The experimental slopes obtained by linear regression analysis of the Stern-Volmer plots in Fig. 1 ranged from 66 liter lipid/mmol plastoquinone in control liposomes to 0.45 liter lipid/mmol plastoquinone in proteoliposomes at 62 wt% protein. This was the typical range of experimental values obtained for the six proteins studied. As is apparent in Fig. 1, experimental slopes $\lesssim 1$ liter lipid/mmol plastoquinone are close to the experimental variability and represent the lower limit of applicability of the pyrene fluorescence–quenching measurement technique.

Estimation of lateral diffusion coefficient

Lateral diffusion coefficients in proteoliposomes were estimated from the slopes of Stern-Volmer plots by the method in reference 8, using the relation,

$$D = \pi(32N_0ht_1f_1)^{-1}[(P^2 + 4m)^{1/2} - P]^2, \qquad (1)$$

where N_0 is Avogadro's number; h is the membrane thickness, assumed to be 4 nm; t_1 is the lifetime of the slower pyrene fluorescence decay component (8); f_1 is a fitting parameter equal to 0.653 (8); P is a parameter obtained by linear interpolation using tables presented in reference 8 and average values of biexponential pyrene monomer fluorescence decay parameters in phosphatidylcholine liposomes from six determinations (data not shown); and m is the experimental slope obtained from linear regression analysis of I^0/I vs. the plastoquinone concentration in the membrane, $[PQ]_m$. Other parameter values are specified in the figure captions.

In proteoliposomes, it is necessary to decide whether or not the protein transmembrane portion should be included in the total membrane volume for the calculation of $[PQ]_m$. Table 1 lists current structural information about the integral membrane proteins considered in the present study, including molecular weights, contents of transmembrane helices, and cross-sectional areas of the protein transmembrane hydrophobic region. In *Rb. sphaeroides* reaction centers (51) and presumably other large protein complexes, the transmembrane alpha helices appear to be closely packed, barring diffusional access by quinones and other lipids. The helix packing is likely to be somewhat variable, as the cross-sectional area per transmembrane helix varies in Table 1 from 0.73 to 2 nm^2, the average being ~1.4 nm^2. However, proteins with smaller hydrophobic volumes, such as cytochrome *f* (45, 46) and gramicidin (53), might not bar diffusional access in the same way. The molecular dimensions and lateral diffusional properties of gramicidin at low gramicidin concentrations are very similar to those of lipid molecules (53), and, thus, gramicidin might not constitute an impenetrable protein domain in the absence of aggregation. To determine the effect of the protein volume in the calculation of plastoquinone concentrations, we estimated diffusion coefficients using two definitions of $[PQ]_m$, as detailed in Appendix A. In the first case (Eq. A1), $[PQ]_m$ was defined as moles of solute per liter of lipid and in the second case (Eq. A3), $[PQ]_m$ was defined as moles of solute per total membrane volume including both the lipid volume and the protein hydrophobic volume.

Fig. 2 shows plots of estimated lateral diffusion coefficients vs. the protein/lipid molar ratio for phosphatidylcholine proteoliposomes containing reaction centers from *Rb. sphaeroides* R-26 mutant (Fig. 2 *A*), spinach cytochrome *bf* complex (Fig. 2 *B*), cytochrome bc_1 from beef heart mitochondria (Fig. 2 *C*), cytochrome oxidase from beef heart mitochondria (Fig. 2 *D*), spinach cytochrome *f* (Fig. 2 *E*), and gramicidin D (Fig. 2 *F*). Lateral diffusion coefficients estimated using Eq. 1 and A1 for $[PQ]_m$ are observed to decrease from $0.8–3 \cdot 10^{-7}$ $cm^2\ s^{-1}$ in control phosphatidylcholine liposomes by an order of magnitude or more at protein/lipid molar ratios $\gtrsim 0.005$. Diffusion coefficients estimated based on the calculations of $[PQ]_m$ using both Eq. A1 and A3, are shown in Figs. 2, *E* and *F*, for cytochrome *f* and gramicidin. The effect of the protein volume is minor for proteoliposomes containing cytochrome *f*, as shown in Fig. 2 *E*, as well as for the other large proteins (not shown). However, in the case of gramicidin, including the protein volume in the calculation of the plastoquinone

TABLE 1 Protein molecular weights, transmembrane helices,* and average cross-sectional membrane areas per protein molecule‡

Protein	Molecular weight	Transmembrane helices* per mole protein	Cross-sectional area per protein molecule‡
	kD		*nm²*
Bacteriorhodopsin from *Halobacterium halobium*	27§ (43)	7‖ (43)	8.75¶ (44)
Cytochrome bc_1 from beef heart mitochondria	250§ (47, 49–52)	12–14‖ (47, 51)	18** (49–51)
Cytochrome *bf* from spinach chloroplasts	96§ (29, 45, 46)	8–10‖ (45, 46)	14‡‡
Cytochrome *f* from spinach chloroplasts	33§ (29, 45, 46)	1‖ (45, 46)	0.8–1.0§§
Cytochrome oxidase from beef heart mitochondria	162‖ (48, 49, 52)	>21‖ (48, 52)	15.5¶ (48)
Gramicidin D	2 (15)	0.5¶¶ (15, 53)	2.0¶¶***
Reaction centers from *Rhodobacter sphaeroides* R-26	100‖ (54)	11¶¶ (54)	19‡‡‡

*Alpha-helices, except for gramicidin, which has the beta-helical conformation.

‡Represents the estimated average protein cross-sectional area normal to the membrane surface, excluding aqueous protein regions not occupying the lipid region of the membrane.

§Estimated from SDS-PAGE migration patterns.

‖Estimated from hydropathy analysis (55).

¶Obtained by electron microscopy and image reconstruction with 2D crystals.

**Calculated Eq. 2, assuming a protein partial specific volume of 0.72 cm^3g^{-1}, the average over the range 0.69–0.75 cm^3g^{-1} typical of proteins (55), and that 30% of the protein occupies a region 5 nm thick, as found by electron microscopy on 2D protein crystals, with a protein molecular weight of 250 kD (49–52).

‡‡Calculated by subtracting 4 nm^2 from the area calculated for cytochrome bc_1, based on the assumption that cytochrome *bf* has 4 fewer transmembrane alpha helices, each assumed to contribute 1.0 nm^2.

§§The average surface area assumed to be occupied by an alpha helix.

‖Obtained from primary amino acid sequences.

¶¶Obtained by x-ray crystallographic analysis of 3D crystals.

***Cross-sectional area of a dimeric gramicidin channel with a 1.6 nm diameter (53).

‡‡‡Estimated average (M. Schiffer, Argonne, IL, personal communication) from 2D projections using the coordinates from x-ray crystallographic analysis.

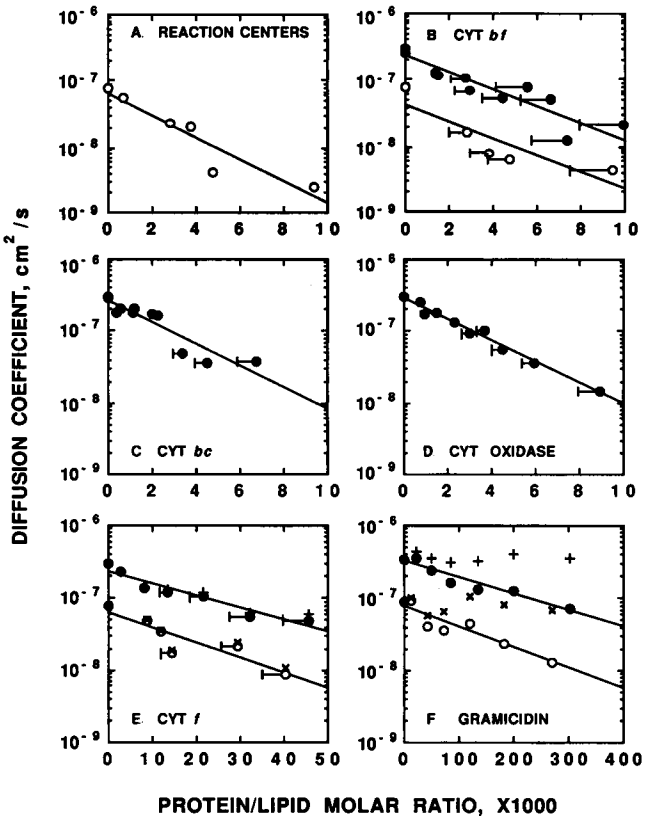

FIGURE 2 The dependence of pyrene fluorescence quenching on the protein composition of soybean phosphatidylcholine proteoliposomes. Plots of the plastoquinone diffusion coefficient as a function of the protein to lipid molar ratio in: proteoliposomes containing reaction centers from *Rhodobacter sphaeroides* (*A*), the cytochrome *bf* complex from spinach chloroplasts (*B*), cytochrome bc_1 from beef heart mitochondria (*C*), cytochrome oxidase from beef heart mitochondria (*D*), cytochrome *f* from spinach chloroplasts (*E*), and gramicidin D (*F*). Circles: Diffusion coefficients estimated assuming that the plastoquinone concentration in the membrane is given by Eq. A1 (i.e., by the number of moles of plastoquinone per liter lipid bilayer). Closed circles represent proteoliposomes prepared by Method A (one experiment in *E*, two experiments in *B–F*) and open circles represent proteoliposomes prepared by Method B (one experiment in *A–F*). Protein/lipid molar ratios were calculated assuming the protein molecular weights listed in Table 1 and a lipid molecular weight of 805 g/mol (40). Bars in B–E: Correction for calculation of protein/lipid molar ratios assuming the values of gram protein/mole determined experimentally and described in Materials and Methods rather than the values in Table 1. (+,x) in E and F: Diffusion coefficients estimated assuming that the plastoquinone concentration in the membrane is given by Eq. A3 (i.e., by the number of moles of plastoquinone per liter membrane including both lipid bilayer and hydrophobic protein regions), for proteoliposomes prepared by Methods A (+) and B(x). (Solid curves) Best-fit single exponential lines. Lipid concentrations were 0.1 mg/ml (*A–E*), and 0.2 mg/ml (*F*). Diffusion coefficients were estimated from Stern-Volmer plots (e.g., Fig. 1) in proteoliposomes using Eq. 1, assuming an interaction radius of 1 nm, a membrane thickness of 4 nm and biexponential pyrene fluorescence decay kinetics ($A_1 \exp(-t/t_1) + A_2 \exp(t/t_2)$ with $A_1 = 0.6192$, $t_1 = 152$ ns, $A_2 = 0.3808$, $t_2 = 67.77$ ns, using the notation of reference 8). The pyrene concentration was 0.3–0.5 μM. Further details are given in the text.

concentration results in estimated lateral diffusion coefficients being nearly independent of the gramicidin concentration. This result would be expected if gramicidin were merely occupying space as a lipid would, diluting plastoquinone by increasing the volume of the bilayer in proteoliposomes, rather than changing the membrane viscosity and hindering diffusion.

As is evident in Figs. 2, *B*, *E*, and *F*, diffusion coefficients estimated in control liposomes containing no protein prepared by Method A ($2–3 \times 10^{-7}$ cm^2 s^{-1}) were similar to those estimated previously (8), whereas those of control liposomes prepared by Method B were systematically lower ($0.7–0.9 \times 10^{-7}$ cm^2 s^{-1}). This difference between the two plastoquinone incorporation procedures may reflect less than complete incorporation via Method B, which involves fusion of pyrene-containing proteoliposomes with plastoquinone-containing liposomes. Incomplete plastoquinone incorporation would result in observation of lower than expected pyrene fluorescence quenching and, thus, an underestimation of diffusion coefficients. Method B did not always result in observable quenching and, in Fig. 2, the degree of fluorescence quenching in measurements using Method B is smaller than expected.

The fluorescence-quenching method results in estimates of the sum of the lateral diffusion coefficients of the probe and quencher (8). However, the pyrene diffusion coefficient is likely to be negligible in comparison to that of plastoquinone. This conclusion is based on the observation that the lateral diffusion coefficient for pyrene in liposomes estimated from studies of the concentration dependence of fluorescence decay kinetics is much lower than values of the order 3×10^{-8} cm^2 s^{-1} obtained in studies of the ratio of monomer to excimer steady-state fluorescence intensities, which are likely to reflect pyrene aggregation rather than collisional excimer formation (37). This value is an order of magnitude smaller than the diffusion coefficient measured by pyrene fluorescence quenching previously (8) or in present studies on liposomes prepared by detergent dilution (Method A). Furthermore, the interpretation of the observed decreases in lateral diffusion as an obstruction or hindrance of lateral mobility by integral membrane proteins is not affected by the relative magnitudes of the pyrene and plastoquinone diffusion coefficients.

The molecular weights listed in Table 1 for the four cytochrome proteins studied here are lower than the assayed values of grams protein per mole presented above in Materials and Methods, which may reflect either a loss of heme during purification, or contamination by other membrane proteins that copurify. The horizontal bars in Figs. 2, *B–E*, indicate the positions the protein/lipid molar ratios would have if calculated assuming the measured values of grams protein/mole cytochrome c_1, *f*, or aa_3, rather than the values in Table 1. Whereas there is

an obvious difference, particularly at higher protein/lipid molar ratios, the assumed protein molecular weights do not significantly affect the overall interpretation of the data, and the values in Table 1 are used in the following analysis.

DISCUSSION

Interpretation of quenching data

The observed decreases in the slope of Stern-Volmer plots with increasing concentration of integral membrane proteins (e.g., Fig. 1) are assumed to reflect a decrease in the rate of collisional quenching of pyrene fluorescence by plastoquinone, and, thus, to correspond to decreases in lateral diffusibility. However, several other possible explanations for the observed decreases would not involve changes in diffusibility. Plastoquinone binding to specific sites on the proteins could reduce the concentration of freely diffusing plastoquinone, leading to a significant decrease in the slope of Stern-Volmer plots. This seems an unlikely cause of the results presented here, in that decreases in the extent of pyrene fluorescence quenching caused by proteins that are known to have quinone binding sites (bacterial reaction centers, cytochrome *bf*, and cytochrome bc_1) were not systematically different from those caused by proteins that lack them (gramicidin, cytochrome *f*, and cytochrome oxidase). Furthermore, specific binding of plastoquinone to protein would produce an apparent onset lag in the fluorescence-quenching ratio at low-plastoquinone concentrations and a positive *x*-intercept in Stern-Volmer plots, approximately equal to the protein concentration (~1 μM for cytochrome *bf* at 50 wt% protein with 0.1 mg/ml phosphatidylcholine). The *x*-intercepts of the Stern-Volmer plots for cytochrome *bf* complex (Fig. 1) and the other proteins studied (data not shown) were zero within experimental error. Nonspecific binding of plastoquinone would also account for the observed decreases in the slopes of Stern-Volmer plots. However, this seems unlikely because quinone molecules appear to be bound stoichiometrically to binding sites on isolated quinone binding proteins (28, 30), i.e., there appears to be no nonspecific binding of quinones, and there is no systematic difference in the results for proteins that have specific quinone binding sites and those that lack them. Other possible causes of the observed decreases in the slopes of Stern-Volmer plots include protein effects on the efficiency of collisional quenching and protein-induced lateral phase separation or other heterogeneity that could be accompanied by differential partition of probe and quencher. These possibilities cannot be discounted without detailed studies of the pyrene fluorescence kinetics and the ultrastructural properties of the samples.

Comparison of results with theoretical models

In addition to numerous Monte Carlo studies (including references 21–23, and 56), several theoretical models have been developed to describe the effect of high concentrations of hydrophobic protein on lateral mobility in membranes (16–20). In these models the dependent variable is considered to be the relative diffusion rate, D^*, defined as the diffusion coefficient measured in proteoliposomes (D) relative to that of control liposomes (D_0), i.e., $D^* = D/D_0$, and the independent variable to be the membrane area fraction occupied by protein, c_P, defined as

$$c_P = \frac{2n_P a_P}{n_L a_L + 2n_P a_P}, \tag{2}$$

with n_P or n_L the number of moles of protein or lipid added to the solution, a_L the cross-sectional area per lipid molecule (0.64 for egg lecithin (42)), and a_P the average cross-sectional area of the hydrophobic region of the protein molecule (Table 1). The factor of 2 in the numerator and in the second term in the denominator of Eq. 2 appears as a result of the contribution of membrane-spanning proteins at both bilayer surfaces and should be omitted from the equation in the case of gramicidin, which forms transmembrane dimers (53). The data of Fig. 2 is replotted in Figs. 3, *A–F*, together with curves calculated according to the theoretical models (16–20). Details of the calculations are given in Appendix B.

Lipid domain models. Lipids adjacent to protein ('annular' lipid) or trapped between two or more proteins can become a significant proportion of the total lipid at high-protein concentrations in proteoliposomes (20). D^* could be affected if mobility in such domains is restricted. Pink et al. (20) developed a model to describe the amount of free and potentially restricted (i.e., annular and trapped) lipids as a function of the protein concentration in proteoliposomes. The model describes the effect on the nuclear magnetic resonance chemical shift but is easily adapted to the description of lateral diffusion rates, as described in Appendix B. Figs. 3, *A–E*, (curves *i*) show theoretical plots of D^* calculated when lipids in restricted domains are totally immobilized and have their maximum theoretical effect. For proteoliposomes containing the larger integral membrane proteins (Figs. 3, *A–E*), it is apparent that restricted lipid domains can at best have very little effect on lateral mobility. In the case of gramicidin (Fig. 3 *F*, curve *ii*), both this model and the following lattice model give predictions in reasonable agreement with the experiment data.

Lattice models. Saxton (16–18) has presented several models of two-dimensional steady-state transport, consid-

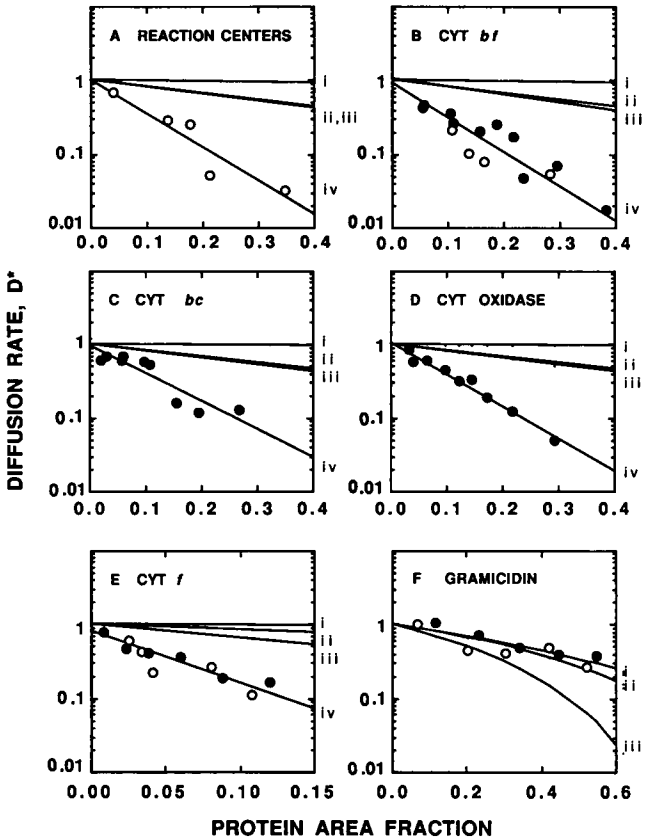

FIGURE 3 Comparison of the experimental results with the predictions of three theoretical models of lateral diffusion in proteoliposomes. The plastoquinone lateral diffusion rate plotted as a function of the protein area fraction in soybean phosphatidylcholine proteoliposomes. Figs. *A–E*: Experimental values of the ratio $D^* = D/D_0$ for proteoliposomes containing reaction centers from *Rhodobacter sphaeroides* (*A*), spinach cytochrome *bf* complex (*B*), beef heart mitochondrial cytochrome bc_1 complex (*C*), beef heart mitochondrial cytochrome oxidase (*D*), and spinach cytochrome *f* (*E*) prepared by Method A (*closed circles*) or B (*open circles*). Theoretical curves calculated using (*i*): the lipid domain model (21, 22) using D^*_{LD} of Eq. B1; (*ii*) a lattice model (16–18) using D^*_L of Eq. B6; (*iii*) the free-volume model (19) using D^*_{FV} of Eq. B10; and (*iv*) the best-fit exponential curve for the experimental data points. Fig. *F*: Experimental values of D^* for gramicidin D proteoliposomes prepared by Method A (*closed circles*) or B (*open circles*). Theoretical curves calculated using: (*i*) the lattice model (16–18) using D^*_L of Eq. B6; (*ii*) the lipid domain model (21, 22) using D^*_{LD} of Eq. B1; and (*iii*) the free-volume model (19), using D^*_{FV} of Eq. B10. Protein area fractions were calculated using Eq. 2 using the protein molecular weights and cross-sectional areas listed in Table 1. Other conditions are as described for Fig. 2. Further details are given in the text and appendices.

ered to be a random walk process on a point lattice, which were used to calculate theoretical curves, as detailed in Appendix B. Figs. 3, *A–E*, show that for the larger proteins in the present study, the theoretical curves (curves *ii*) display a weaker dependence on the protein content of proteoliposomes than is observed experimentally (curves *iv*), consistent with the finding that lipid diffusion rates measured by FPR in bacteriorhodopsin (14) proteoliposomes display a stronger dependence on the protein concentration than is predicted by theory (17). However, the theoretical prediction seems to be in better agreement with the data for gramicidin (Fig. 3 *F*, curve *i*) in the present study than was found previously (17), due to different values assumed for the gramicidin cross-sectional area (1.13 nm^2 [15, 17] vs. 2 nm^2 determined by x-ray studies [53]).

Free-volume model. Free-volume models envision proteins or lipids as hard disks and diffusion as occurring by a series of hops of disks into neighboring free space (holes). According to the model developed by O'Leary (19), the relative diffusion rate D^* depends on the work, W, required to create the free space, and W has an explicit protein concentration dependence, as detailed in Appendix B. Calculations of theoretical curves of D^* for the free volume model are presented in Figs. 3, A–F, (curves *iii*). As with the preceding two theories, it is evident in the case of the larger proteins in Figs. 3, A–E, that the free-volume model predicts a much weaker dependence of lateral mobility on the protein concentration than that observed in the present studies (curves *iv*). However, the model predicts that gramicidin will have a greater effect on lateral mobility than is observed experimentally, particularly at area fractions above 0.4 (Fig. 3 *F*).

As is apparent in Fig. 3, a 10-fold decrease in the diffusion coefficient occurred at area fractions between 0.16 and 0.26 for all of the proteins except gramicidin. All three theoretical models considered here predict a much weaker dependence of lateral diffusion on the protein concentration in proteoliposomes than is observed using the pyrene fluorescence–quenching method. The maximum combined effect of the three models, i.e., the product $D^*_T = D^*_{LD} D^*_L D^*_{FV}$ from Eqs. B1–B10 in Appendix B, is also too small to acount for the observed effect of protein on lateral mobility in Fig. 3, *A–E*.

Impact of protein hydrophobicity on lateral mobility

Fig. 4 shows that the effectiveness of a particular protein in decreasing lateral mobility is strongly correlated with the size of its hydrophobic region. The volumes of the hydrophobic regions of cytochrome *bf*, *Rhodobacter sphaeroides* reaction centers, cytochrome bc_1, and cytochrome oxidase are 15–20 times as large as that of cytochrome *f* and the gramicidin transmembrane dimer (4 nm^3), as calculated using the data in Table 1 and Eq. A4 in Appendix A. Fig. 4 *A* shows that this corresponds to a nearly 15–20-fold increase in the slope of the best fit exponential curves in Fig. 2 (Fig. 4 *A*). However, Fig. 4 *B* shows that there is no apparent correlation between the

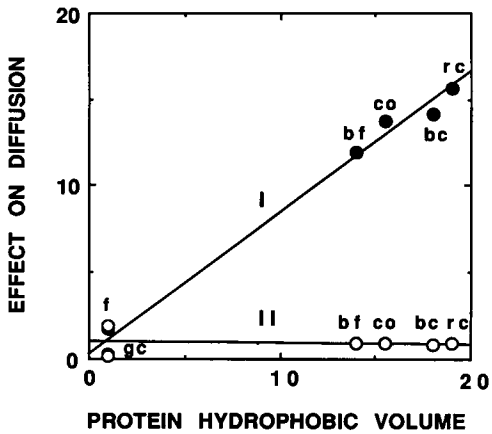

FIGURE 4 Effect of increasing protein hydrophobic volume on ability to obstruct lateral mobility. (I, *A–F*) The ratio of the slopes of best fit lines in Fig. 2, *A–F*, respectively, to the average of the slopes for cytochrome *f* in Fig. 2 *E* and gramicidin in Fig. 2 *F*. The solid line is the best-fit straight line through the data points ($y = 0.18 + 0.82x$, with a correlation coefficient of $r = 0.995$). (II, *A–F*) The ratio of the slopes of the best fit lines in Fig. 3, *A–F*, respectively, to the average of the slopes for cytochrome *f* in Fig. 3 *E* and gramicidin in Fig. 3 *F*. The solid line is the best-fit straight line through the data points ($y = 1.01 - 0.007x$, with a correlation coefficient of $r = 0.11$). Hydrophobic volumes were calculated as $a_P h$, with a_P the average cross-sectional area of the hydrophobic region of the protein molecule (Table 1), and h the membrane thickness, and plotted in units of the hydrophobic volumes of gramicidin and cytochrome *f* (4 nm^3). Slopes obtained for Methods A and B in Figs. 2 and 3 were averaged.

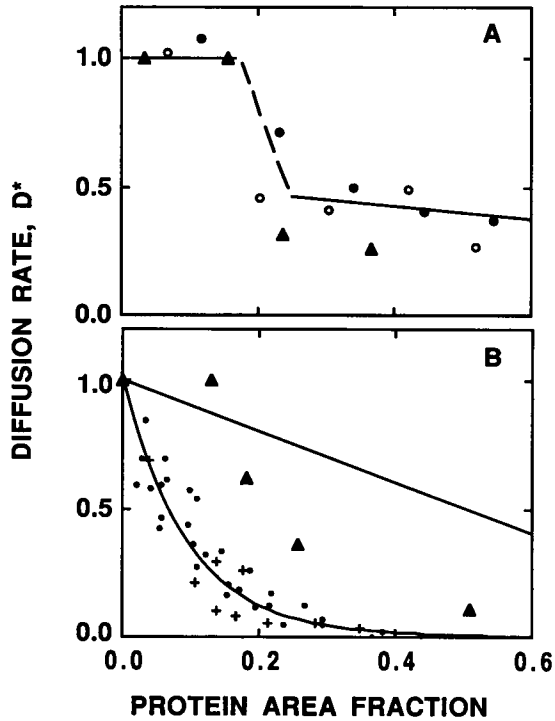

FIGURE 5 Comparison of present results with previous studies of lipid diffusion in proteoliposomes. Plots of D^* as a function of the protein area fraction. (*A*) Experimental values of D^* obtained in the present study estimated assuming that the plastoquinone concentration in the membrane is given by Eq. A1 (i.e., by the number of moles of plastoquinone per liter lipid bilayer), for proteoliposomes prepared by Method A (*closed circles*) or Method B (*open circles*) replotted from Fig. 3 *F*. D^* in dimyristoyl phosphatidylcholine-gramicidin proteoliposomes obtained in FPR measurements by Tank et al. (15) (▲). (*B*) Experimental values of D^* obtained in the present study by Method A (*dots*) or B(+), replotted from Figs. 3, *A–D*. Experimental values of D^* in dimyristoyl phosphatidylcholine-bacteriorhodopsin proteoliposomes obtained in FPR measurements by Peters and Cherry (14) (▲). Theoretical curve for D^* at time zero from Eq. 3 (*upper line*) and best-fit exponential curve for the data points (*lower curve*). Area fractions were calculated as described for Fig. 2, making allowance when appropriate for the different molecular weights of dimyristoyl phosphatidylcholine and soybean phosphatidylcholine.

hydrophobic volume and the slope of the best fit exponential curves in Fig. 3, supporting the use of the protein area fraction as the independent variable in theoretical studies.

Comparison with FPR measurements

A comparison of the present results with values of D^* from FPR measurements on gramicidin (15) and bacteriorhodopsin (14) proteoliposomes is presented in Fig. 5. Protein area fractions for gramicidin and bacteriorhodopsin were calculated using Eq. 2, assuming the molecular weights and cross-sections listed in Table 1. Fig. 5 *A* presents a plot of D^* for gramicidin from Fig. 3 *F* together with values obtained by FPR for lipid diffusion in dimyristoyl phosphatidylcholine-gramicidin proteoliposomes (15). The two data sets are in close agreement, showing that D^* is independent of the gramicidin content <0.15-area fraction protein, followed by a sharp dependence in the region 0.15–0.25 area fraction and a weak dependence >0.25 area fraction. A possible interpretation of this data is that at area fractions < 0.15 gramicidin is not acting as an obstacle to diffusion in the same way as the larger proteins, but is merely diluting the membrane space. Both the sharp transition in the region 0.15–0.25 area fraction and the weak dependence on gramicidin content >0.25 area fraction may reflect aggregation or a lack of protein incorporation.

Fig. 5 *B* is a plot of all the data points from Figs. 3, *A–D*, together with the relative diffusion rate D^* based on measurements of lateral diffusion coefficients for bacteriorhodopsin in dimyristoyl-phosphatidylcholine proteoliposomes (14). It is apparent in Fig. 5 *B* that the proteins in the present study have a significantly stronger effect on D^* than does bacteriorhodopsin. This may reflect systematic differences between bacteriorhodopsin and the proteins studied here, or between the FPR and pyrene fluorescence–quenching methods. The lateral diffusion

coefficients reported here remain significantly higher than the control values reported for lipid diffusion in dimyristoyl phosphatidylcholine liposomes (14, 15), indicating a systematic difference between FPR and fluorescence quenching or between dimyristoyl phosphatidylcholine and soybean phosphatidylcholine. A similar disparity has been found in electron spin resonance (esr) studies (57, 58). The lateral diffusion coefficients measured for phospholipids by esr imaging (57), which involves observing the relaxation of concentration gradients on a size scale comparable to that of FPR experiments, are about a factor of two higher than those measured by FPR, possibly reflecting that the bulkier active groups used in FPR probes are affecting diffusion. Moreover, lateral diffusion coefficients measured by Heisenberg spin exchange (58), which involves collisional interactions on a timescale similar to that of fluorescence-quenching experiments, appear to be systematically higher than those obtained by esr imaging. Thus, according to two independent techniques, optical and esr spectroscopy, collisional processes apparently give higher measurements of diffusion coefficients than those based on observing the relaxation of concentration gradients.

There have been several recent suggestions (10, 22, 56) that systematic differences between the fluorescence quenching and FPR measurements may result from the measurement of lateral diffusion over longer distances in FPR experiments than in fluorescence-quenching experiments, and this may also supply to the esr measurements. Saxton has studied D^* in Monte Carlo simulations and found it to be time dependent, falling from its value at time zero,

$$D^*(t_0) = 1 - c_P, \tag{3}$$

to a lower steady-state value within 5–10 diffusive steps (56). Thus, the diffusion coefficient may not achieve a steady-state value within the collision time and would appear to be higher in shorter-range measurements than in longer-range measurements, consistent with results.

It has been suggested (10, 23, 56) that long-range diffusion in FPR measurements may appear to be more obstructed by integral membrane proteins than shorter range diffusion as measured in quenching studies. However, the opposite trend is evident in Fig. 5 *B*, i.e., the effect of protein is more profound in fluorescence-quenching measurements than in FPR measurements: the FPR results for bacteriorhodopsin lie between the curve plotted for Eq. 3 and the experimental data points in Fig. 5 *B*. Thus, time dependence of the diffusion coefficient cannot apparently account for the differences between the fluorescence quenching and FPR results in Fig. 5 *B*. It is possible that this disagreement and the difference between the fluorescence quenching and FPR results plotted in Fig. 5 *B* result from the probes and quenchers used in the various experiments having different interaction radii, distributions normal to the membrane surface, etc. The difference between the results of FPR and fluorescence-quenching measurements plotted in Fig. 5 *B* could reflect a more profound effect of protein on the mobility of plastoquinone than on that of the fluorescence lipids used in FPR studies, which have fatty acid chains less than half as long as the phytol tail of plastoquinone. By similar reasoning, protein would be expected to have a smaller effect on the mobility of the fluorescence quencher used in the studies of submitochondrial particles, ubiquinone-3, which has a shorter hydrocarbon tail than those of plastoquinone-9 and ubiquinone-10, i.e., 15, rather than 45 or 50 carbon atoms, respectively, consistent with observation (7). However, this should also apply to the ubiquinone analogue used in the FPR measurements in the mitochondrial inner membrane that has a short 10 carbon atom hydrocarbon tail, inconsistent with the observation of a profound effect of protein (9).

Both the disparity between the FPR and the pyrene fluorescence–quenching results in Fig. 5 and the disparity between theory and experiment in Fig. 3 could be explained by invoking lipid protein or quinone/protein interactions as an important mechanism of obstruction by proteins in membranes. A distance-dependent interaction potential would give rise to a dependence on the protein concentration that could account for the differences between the theoretical and experimental curves. This would also be consistent with the finding that it is necessary to include protein/lipid interactions in excess of hard-sphere interactions to bring Monte Carlo simulations into agreement with experimental values (17, 21, 22) as well as recent findings that the activational barrier to diffusion measured by FPR in mitochondrial inner membranes decreases with increasing protein dilution (10). However, quinone/protein interactions are a problematical explanation for the protein effects reported here, unless the quinone is reporting on more generalized lipid/protein interactions: according to the Einstein relation, plastoquinone can undergo a root mean square displacement of 2 $(Dt)^{1/2}$, or roughly 0.5 nm within the pyrene fluorescence lifetime of 100 ns if the diffusion coefficient is 10^{-8} cm^{-1} s^2, a distance much smaller than the average protein/protein distance at even the highest protein concentrations we studied. This seems inconsistent with a mechanism by which plastoquinone mobility is obstructed by means of direct, e.g., collisional or binding, interaction of plastoquinone with protein, but consistent with an effect of protein on some more delocalized property, such as lipid packing, that could affect membrane viscosity.

The results presented here help to resolve the discrepancy between quinone diffusion coefficients estimated to

be in the region of 1–2 × 10^{-7} cm^2 s^{-1} by the probe fluorescence–quenching method (6–8) and a value that was measured by FPR in mitochondrial inner membrane that was two orders of magnitude lower (9). As the latter membrane contains >70 wt% protein (13), one would expect to see a profound decrease in the quinone lateral diffusion rate, based on the FPR results and the results presented here. The results presented here as well as FPR results in mitochondrial membranes (9, 10) and proteoliposomes (14, 15) are in apparent disagreement with probe fluorescence–quenching measurements of quinone diffusion coefficients in submitochondrial particles that are of the same order of magnitude as in pure lipid vesicles (7). Whereas the reason for this disagreement is presently unknown, the weight of the evidence seems to favor the view that plastoquinone as well as ubiquinone and the ubiquinone analogues that have been studied behave like typical lipids both in the magnitude of their lateral diffusion coefficients and in the effect of hydrophobic proteins on lateral mobility.

APPENDIX A. CALCULATION OF PLASTOQUINONE CONCENTRATION IN THE MEMBRANE

The concentration of plastoquinone in the membrane in proteoliposomes may be defined either as moles of plastoquinone per liter of lipid or as moles of plastoquinone per liter of membrane bilayer including both the lipid and the protein hydrophobic volume.

In the first case, the lipid bilayer is considered to be the solvent in which plastoquinone and pyrene are solutes and the protein hydrophobic region is considered to form a domain impenetrable to both lipids and solutes, so that

$$[PQ]_m = n_{PQ}/V_L, \tag{A1}$$

with n_{PQ} the number of moles of plastoquinone added to the solution, and V_L the volume of the lipid bilayer region, approximated throughout the present analysis by

$$V_L \sim n_L W_L/\rho_L, \tag{A2}$$

with n_L the number of moles of lipid added to the solution, W_L the lipid molecular weight (assumed throughout to be 805 g/mol for soybean phosphatidylcholine, as for egg lecithin [41]), and ρ_L the lipid density (assumed throughout to be 1,000 g/liter for soybean phosphatidylcholine, as for egg lecithin [41]), all expressed in appropriate units.

In the second case, with the exception of cytochrome bc_1, the volume of the protein domain is included in the membrane bilayer volume for the calculation of plastoquinone concentrations, so that

$$[PQ]_m = n_{PQ}/(V_L + V_P), \tag{A3}$$

with n_{PQ} as defined for Eq. A1, V_L as defined by Eq. A2, and V_P the total volume of the protein hydrophobic region, approximated in the present analysis by

$$V_P \sim n_P a_P h N_0, \tag{A4}$$

with n_P the number of moles of protein, a_P the average cross-sectional area of the hydrophobic region of the protein molecule, h the membrane thickness, and N_0 Avogadro's number, all in appropriate units. For cytochrome bc_1, V_P was calculated as $V_P \sim n_P W_P/\rho_P$, with W_P the protein molecular weight, and ρ_P the protein density, assumed to be 1,389 g/liter as in Table 1, note **.

Eqs. A1 and A3 assume negligible solubilities for plastoquinone and lipid except in membrane bilayers. The cross-sectional areas a_P and a_L are not rigorously defined quantities, as both the transmembrane portions of the proteins and the lipid acyl chains in phosphatidylcholine are heterogeneous in shape and size. The values used here are assumed to be average values and to correspond to minimal, hard-core cross-sectional areas. The membrane volume contributed by plastoquinone and pyrene are neglected in Eqs. A1 and A3.

APPENDIX B

The theoretical analysis used to generate curves *i–iii* in Fig. 3, *A–F*, is presented here, including specification of parameter values used in the calculations.

Lipid domain models

According to the analysis of Pink et al. (20), the diffusion coefficient has a concentration dependence of the form

$$D^*_{LD}(c_P) = A_F(c_P)D^*_F + A_A(c_P)D^*_A + A_T(c_P)D^*_T, \tag{B1}$$

where D^*'s denote ratios D_{LD}/D_0, D_F/D_0, D_A/D_0, and D_T/D_0, respectively; D_0 is the diffusion coefficient in the absence of protein, D_F is the diffusion coefficient of plastoquinone in the free (not annular or trapped) lipid domain, D_A is the diffusion coefficient of annular plastoquinone, and D_T is the diffusion coefficient of plastoquinone trapped between two or more protein molecules; A_F, A_A and A_T denote the fractions of the total plastoquinone population that exist in the free, annular, or trapped lipid domains, respectively, and are given by

$$A_F = (1 - c_P)\left[\frac{W_P}{2W_L\xi} + \frac{\pi}{4}(R_P/R_L) + 1)c_P\right] \tag{B2}$$

$$A_A = c_P(1 - c_P)\frac{\pi}{2}(R_P/R_L + 1) \tag{B3}$$

$$A_T = 3n_2c_P^2 + 2n_3c_P^3, \tag{B4}$$

with c_P the protein area fraction as defined for Eq. 2, W_P and W_L the protein and lipid molecular weights defined in Appendix A, ξ a site filling factor roughly equal to 0.9 (20), and with n_2 or n_3 the respective number of lipid molecules that can be trapped between two or three protein molecules. For our calculation we set $n_2 = n_3 = 1$; Pink et al. (20) used values between 0.5 and 2 for molecules as diverse as gramicidin and cytochrome oxidase, respectively.

Pink et al. (20) assumed that the protein/lipid area ratio was given by the molecular weight ratio and that the protein area fraction is equal to the protein weight fraction. We modified this by defining the protein area fraction as in Eq. 2 and by assuming that

$$R_P/R_L = (a_P/a_L)^{1/2}, \tag{B5}$$

with R_L or R_P the respective lipid or protein 'hard-core' radii and a_P as defined in Appendix A, and a_L the lipid 'hard-core' radius, assumed to be 0.64 nm^2 as for egg lecithin (42).

Lattice models

According to Saxton's analysis (17), diffusion in the presence of mobile proteins has a concentration dependence of the form (18)

$$D_L^*(c_P, \gamma) = (1 - c_P)F(c_P, \gamma), \tag{B6}$$

with $F(c_P, \gamma)$ the correlation factor

$$F(c_P, \gamma) = [2\gamma(1 - c_P)f]^{-1} \times [[[(1 - \gamma)(1 - c_P)f + c_P]^2 + 4\gamma(1 - c_P)f^2]^{1/2} - [(1 - \gamma)(1 - c_P)f + c_P]] \tag{B7}$$

and

$$f = \frac{[1 - \alpha]}{[1 + (2\gamma - 1)\alpha]}, \tag{B8}$$

where α is a constant dependent on the lattice geometry for which we assumed the square-lattice value of 0.36338 (17), and γ is the ratio of the lipid and protein random walk jump frequencies (17), assumed for the present analysis to be equal to the ratio of the lipid and protein lateral diffusion coefficients. Based on Saffman's equation (59) we wrote this ratio as

$$\gamma = \frac{\ln \frac{\eta h}{\eta_W R_L} - 0.5772}{\ln \frac{\eta h}{\eta_W R_L} - 0.5772}, \tag{B9}$$

in which η and η_W are the membrane and water viscosity, h is the membrane thickness, and the other symbols are as previously defined. The value $\eta/\eta_W = 100$ was used in the calculation.

Free-volume model

According to O'Leary's analysis (19), the dependence of W on the protein concentration results in a concentration dependence of the relative diffusion rate of the form

$$D_{FV}^* = (1 - c_P) \exp\left(\frac{-\zeta c_P}{1 - c_P}\right), \tag{B10}$$

where

$$\zeta = \frac{2\gamma_P R_L}{\sigma R_P}, \tag{B11}$$

γ_p is a semiempirical constant of the order 1 or less, and σ is a lipid packing parameter

$$\sigma = \frac{a_L}{a_L + a_F} \tag{B12}$$

in which a_L is as defined for Eq. B5, and a_F is the free area per lipid molecule. In O'Leary's analysis (19), σ is in the region of 0.5–0.6 for tight to loose packing. The other symbols are as defined previously. The present calculation used the relation $\xi \sim 3.6\ R_P/R_L$, obtained assuming that $\gamma_P = 1$ and $\sigma = 0.55$.

We are grateful to Dr. Michael Saxton of University of California-Davis for useful discussions and for communicating results before publication. We thank Dr. William Cramer of Purdue University and Dr. Marianne Schieffer of Argonne National Laboratory for helpful discussions. Negative stain transmission electron microscopy studies were carried out at the center for Electron Microscopy at the University of Illinois.

This work was supported in part by the Photosynthesis Program of the Competitive Grants Office of the United States Department of Agriculture (grant no. AG86-CRCR-1-1987 and 88-37130-3366).

Received for publication 17 July 1989 and in final form 2 July 1990.

REFERENCES

1. Singer, S. J. and G. L. Nicolson. 1972. The fluid mosaic model of the structure of cell membranes. *Science (Wash. DC).* 175:720–731.
2. Axelrod, D. 1983. Lateral motion of membrane proteins and biological function. *J. Membr. Biol.* 75:1–10.
3. Whitmarsh, J. 1986. Moble electron carriers in thylakoids. *In* Photosynthesis III. Vol. 19. Encyclopedia of Plant Physiology. L. A. Staehelin and C. Arntzen, editors. Springer-Verlag GmbH, Heidelberg, FRG. 508–525.
4. Cherry, R. 1979. Rotational and lateral diffusion of membrane proteins. *Biochim. Biophys. Acta.* 559:289–327.
5. Chance, B., M. Erecinska, and G. K. Radda. 1975. 12-(9-Anthroyl)stearic acid, a fluorescent probe for the ubiquinone region of the mitochondrial membrane. *Eur. J. Biochem.* 54:521–529.
6. Fato, R., M. Battino, G. Parenti-Castelli, and G. Lenaz. 1985. Measurement of the lateral diffusion coefficients of ubiquinones in lipid vesicles by fluorescence quenching of 12-(9-anthroyl)stearate. *FEBS (Fed. Eur. Biochem. Soc.) Lett.* 179:238–242.
7. Fato, M. Battino, M. Degli-Esposti, G. Parenti-Castelli, and G. Lenaz. 1986. Determination of partition and lateral diffusion coefficients of ubiquinones by fluorescence quenching of *n*-(9-anthroyloxy)stearic acids in phospholipid vesicles and mitochondrial membranes. *Biochemistry.* 25:3378–3390.
8. Blackwell, M. F., K. Gounaris, S. J. Zara, and J. Barber. 1987. A method for estimating lateral diffusion coefficients in membranes from steady-state fluorescence quenching studies. *Biophys. J.* 51:735–744.
9. Gupte, S., E. Wu, L. Hoechli, M. Hoechli, K. Jacobson, A. E. Sowers, and C. R. Hackenbrock. 1984. Relationship between lateral diffusion, collision frequency and electron transfer of mitochondrial inner membrane oxidation-reduction components. *Proc. Natl. Acad. Sci. USA.* 81:2606–2610.
10. Chazotte, B., and C. R. Hackenbrock. 1989. Lateral diffusion as a rate-limiting step in ubiquinone-mediated mitochondrial electron transport. *J. Biol. Chem.* 264:4978–4985.
11. Millner, P. A., and J. Barber. 1984. Plastoquinone as a mobile redox carrier in the photosynthetic membrane. *FEBS (Fed. Eur. Biochem. Soc.) Lett.* 169:1–6.
12. Vaz, W. L. C., F. Goodsaid-Zalduondo, and K. Jacobson. 1984. Lateral diffusion of lipids and proteins in bilayer membranes. *FEBS (Fed. Eur. Biochem. Soc.) Lett.* 174:199–207.
13. Guidotti, G. 1972. Membrane proteins. *Annu. Rev. Biochem.* 41:731–752.
14. Peters, R., and R. J. Cherry. 1982. Lateral and rotational diffusion of bacteriorhodopsin in lipid bilayers: experimental test of the

Saffman-Delbrueck equations. *Proc. Natl. Acad. Sci. USA.* 79:4317–4321.

15. Tank, D. W., E. S. Wu, P. R. Meers, and W. W. Webb. 1982. Lateral diffusion of gramicidin C in phospholipid multibilayers. Effects of cholesterol and high gramicidin concentration. *Biophys. J.* 40:129–135.
16. Saxton, M. J. 1982. Lateral diffusion in an archipelago. Effects of impermeable patches on diffusion in a cell membrane. *Biophys. J.* 39:165–173.
17. Saxton, M. J. 1987. Lateral diffusion in an archipelago. The effect of mobile obstacles. *Biophys. J.* 52:989–997.
18. Van Beijeren, H., and R. Kutner. 1985. Mean square displacement of a tracer particle in a hard-core lattice gas. *Phys. Rev. Lett.* 55:238–241.
19. O'Leary, T. J. 1987. Lateral diffusion of lipids in complex biological membranes. *Proc. Natl. Acad. Sci. USA.* 84:429–433.
20. Pink, D. A., A. Georgallas, and D. Chapman. 1981. Intrinsic proteins and their effect upon lipid hydrocarbon chain order. *Biochemistry.* 20:7152–7157.
21. Pink, D. A. 1985. Protein lateral movement in lipid bilayers. Simulation studies of its dependence upon protein concentration. *Biochim. Biophys. Acta.* 818:200–204.
22. Pink, D. A., D. J. Laidlaw, and D. M. Chisholm. 1986. Protein lateral movement in lipid bilayers. Monte Carlo simulation studies of its dependence upon attractive protein-protein interactions. *Biochim. Biophys. Acta.* 863:9–17.
23. Eisinger, J., J. Flores, and W. P. Petersen. 1986. A milling crowd model for local and long-range obstructed lateral diffusion. Mobility of excimeric probes in the membrane of intact erythrocytes. *Biophys. J.* 49:987–1001.
24. Minton, A. P. 1989. Lateral diffusion of membrane proteins in protein-rich membranes. *Biophys. J.* 55:805–808.
25. Abney, J. R., B. A. Scalettar, and J. C. Owicki. 1989. Self diffusion of interacting membrane proteins. *Biophys. J.* 55:817–833.
26. Blackwell, M. F., and J. Whitmarsh. 1989. Plastoquinone diffusion in proteoliposomes studied by pyrene fluorescence quenching. *In* Photosynthesis. Molecular Biology and Bioenergetics. G. S. Singhal, J. Barber, R. A. Dilley, Govindjee, R. Haselkorn, and P. Mohanty, editors. Narosa Publishing House, New Delhi. 225–237.
27. Hildreth, J. E. K. 1982. *N*-D-Gluco-*N*-methylalkanamide compounds, a new class of non-ionic detergents for membrane biochemistry. *Biochem. J.* 207:363–366.
28. Maroti, P., and C. A. Wraight. 1988. Flash-induced H+ binding by bacterial photosynthetic reaction centers: composition of spectrophotometric and conductimetric methods. *Biochim. Biophys. Acta.* 934:314–328.
29. Ho, K. K., and D. W. Krogman. 1980. Cytochrome *f* from spinach and cyanobacteria. Purification and characterization. *J. Biol. Chem.* 255:3855–3861.
30. Hauska, G. 1986. Preparations of electrogenic, proton-transporting cytochrome complexes of the b_6f-type (chloroplasts and cyanobacteria) and bc_1-type. *Methods Enzymol.* 126:271–285.
31. Hartzell, C. R., H. Beinert, B. F. van Gelder, and T. E. King. 1978. Preparation of cytochrome oxidase from beef heart. *Methods Enzymol.* 53:54–66.
32. Crane, F. L. 1959. Quinones with coenzyme Q activity from alfalfa. *Plant Physiol. Bethesda.* 34:546–551.
33. van Gelder, B. F. 1966. On cytochrome *c* oxidase. I. The Extinction Coefficients of cytochrome *a* and cytochrome a_3. *Biochim. Biophys. Acta.* 118:36–46.
34. Whitmarsh, J., and D. R. Ort. 1984. Stoichiometries of electron transport complexes in spinach chloroplasts. *Arch. Biochem. Biophys.* 231:378–389.
35. Rosevear, P., T. VanAken, J. Baxter, and S. Ferguson-Miller. 1980. Alkyl glycoside detergents: a simpler synthesis and their effects on kinetic and physical properties of cytochrome *c* oxidase. *Biochemistry.* 19:4108–4115.
36. Bensadoun, A., and D. Weinstein. 1976. Assay of proteins in the presence of intefering materials. *Anal. Biochem.* 70:241–250.
37. Blackwell, M. F., K. Gounaris, and J. Barber. 1986. Evidence that pyrene excimer formation in membranes is not diffusion controlled. *Biochim. Biophys. Acta.* 858:221–234.
38. Suchy, S. E., P. K. Vinson, and A. Walters. 1989. Solubility properties of the acyl methylglucamide detergents. *Biophys. J.* 55:322a. (Abstr.)
39. Helenius, A., and K. Simons. 1975. Solubilization of membranes by detergents. *Biochim. Biophys. Acta.* 415:29–79.
40. Lichtenberg, D. 1985. Characterization of the solubilization of lipid bilayers by surfactants. *Biochim. Biophys. Acta.* 821:470–478.
41. Newman, G. C., and C.-h. Huang. 1975. Structural studies on phosphatidylcholine-cholesterol mixed vesicles. *Biochemistry.* 14: 3363–3370.
42. Bar, R. S., D. W. Deamer, and D. G. Cornwell. 1966. Surface area of human erythrocyte lipids: reinvestigation of experiments on plasma membrane. *Science (Wash. DC).* 153:1010–1012.
43. Engelman, D. M., T. A. Steitz, and A. Goldman. 1986. Identifying nonpolar transbilayer helices in amino acid sequences of membrane proteins. *Annu. Rev. Biophys. Biophys. Chem.* 15:321–353.
44. Henderson, R., and P. N. T. Unwin. 1975. Three-dimensional model of purple membrane obtained by electron microscopy. *Nature (Lond.).* 257:28–32.
45. Willey, D. L., and J. C. Gray. 1988. Synthesis and assembly of the cytochrome *b–f* complex in higher plants. *Photosynth. Res.* 17:125–144.
46. O'Keefe, D. P. 1988. Structure and function of the chloroplast cytochrome *bf* complex. *Photosynth. Res.* 17:189–216.
47. Gonzalea-Halphen, D., M. A. Lindorfer and R. A. Capaldi. 1988. Subunit arrangement in beef heart complex III. *Biochemistry.* 27:7021–7031.
48. Capaldi, R. A., S. Takamiya, Y.-Z. Zhang, D. Gonzalez-Halphen, and W. Yanamura. 1987. Structure of cytochrome-*c* oxidase. *Curr. Top. Bioenerg.* 15:91–112.
49. Leonard, K., P. Wingfield, T. Arad, and H. Weiss. 1981. Three-dimensional structure of ubiquinol: cytochrome *c* reductase from *Neuspora* mitochondria determined by electron microscopy of membrane crystals. *J. Mol. Biol.* 149:259–274.
50. Karlsson, B., S. Hovmoller, H. Weiss, and K. Leonard. 1983. Structural studies of cytochrome reductase. *J. Mol. Biol.* 165:287–302.
51. Weiss, H. 1987. Structure of mitochondrial ubiquinol-cytochrome-*c* reductase (complex III). *Curr. Top. Bioenerg.* 15:67–90.
52. Hatefi, Y. 1985. The mitochondrial electron transport and oxidative phosphorylation system. *Annu. Rev. Biochem.* 54:1015–1069.
53. Wallace, B. A., and K. Ravikumar. 1988. The gramicidin pore: crystal structure of a cesium complex. *Science (Wash. DC).* 241:182–187.
54. Allen, J. P., G. Feher, T. O. Yeates, H. Komiya, and D. C. Rees.

1987. Structure of the reaction center from *Rhodobacter sphaeroides* R-26: the protein subunits. *Proc. Natl. Acad. Sci. USA.* 84:6162–6166.

55. Cantor, C. R., and P. R. Schimmel. 1980. Biophysical Chemistry. Freeman Publications, San Francisco. 554.

56. Saxton, M. J. 1989. Lateral diffusion in an archipelago. The distance dependence of the diffusion coefficient. *Biophys. J.* 56:615–622.

57. Cleary, D. A., Y.-K. Shin, D. J. Schneider, and J. H. Freed. 1988. Rapid determination of translational diffusion coefficients using ESR imaging. *J. Magn. Reson.* 474–492.

58. Nayeem, A., S. B. Rananavare, V. S. S. Sastry, and J. H. Freed. 1989. Heisenberg spin exchange and molecular diffusion in liquid crystals. *J. Chem. Phys.* 91:6887–6905.

59. Saffman, P. G. 1976. Brownian motion in thin sheets of viscous fluid. *J. Fluid Mech.* 73:593–602.